General Disclaimer

One or more of the Following Statements may affect this Document

- This document has been reproduced from the best copy furnished by the organizational source. It is being released in the interest of making available as much information as possible.

- This document may contain data, which exceeds the sheet parameters. It was furnished in this condition by the organizational source and is the best copy available.

- This document may contain tone-on-tone or color graphs, charts and/or pictures, which have been reproduced in black and white.

- This document is paginated as submitted by the original source.

- Portions of this document are not fully legible due to the historical nature of some of the material. However, it is the best reproduction available from the original submission.

NASA TECHNICAL MEMORANDUM

NASA TM X-73443

NASA TM X-73443

BOUNDARY LAYER THICKNESS EFFECT ON BOATTAIL DRAG

by B. J. Blaha, R. Chamberlin, and L. J. Bober
Lewis Research Center
Cleveland, Ohio 44135

TECHNICAL PAPER to be presented at Twelfth Propulsion Conference cosponsored by the American Institute of Aeronautics and Astronautics and the Society of Automotive Engineers
Palo Alto, California, July 26-29, 1976

BOUNDARY LAYER THICKNESS EFFECT ON BOATTAIL DRAG

by B. J. Blaha, R. Chamberlin, and L. J. Bober
Lewis Research Center
Cleveland, Ohio 44135

E-8797

ABSTRACT

A combined experimental and analytical program has been conducted at the NASA Lewis Research Center, to investigate the effects of boundary layer changes on the flow over high angle boattail nozzles. The tests were run on an isolated axisymmetric sting mounted model. Various boattail geometries were investigated at high subsonic speeds over a range of boundary layer thicknesses. In general, boundary layer effects were small at speeds up to Mach 0.8. However, at higher speeds significant regions of separated flow were present on the boattail. When separation was present large reductions in boattail drag resulted with increasing boundary layer thickness. The analysis predicts both of these trends.

INTRODUCTION

One of the more controversial topics under discussion in the industry is the effect of Reynolds number on the flow over high angle military-type boattail nozzles (Refs. 1 to 13). The subject was brought to light several years ago as a result of a series of installed boattail studies done both in flight and on wind tunnel models at NASA Lewis (Refs. 1 to 5). Because of the unexpected results that were observed, additional tests were conducted by other organizations (Refs. 6 to 13). Many of these investigations were done on isolated models thereby eliminating installation effects. A series of AGARD boattail geometries were defined and tested in various facilities throughout the NATO countries (Refs. 6 to 8) using several techniques to vary the effective Reynolds number. The results from these tests have generally been conflicting. Data obtained in the Langley Cryogenic Wind Tunnel (Refs. 9 and 10) indicate that there is no significant

effect on boattail drag of varying unit Reynolds number for both isolated and installed configurations. Isolated data from the Lockheed-Georgia Compressible Flow Facilities (Ref. 9) indicate, however, that there is an effect of varying unit Reynolds number. Lastly, the data obtained in facilities where the effective Reynolds number was varied artificially (i.e. by changes in model length or by blowing the boundary layer) indicate that there is an effect of boundary layer thickness for some geometries and aerodynamic conditions. Because of these results, it became evident that eliminating the installation effects did not answer all of the questions, and the problem was still complex with other factors besides Reynolds number influencing the end result.

Figure 1 presents some of the complex factors which can influence boattail drag. These include: boundary layer thickness and velocity profile approaching the boattail, shocks with induced separation, geometry induced separation, and jet effects. To further investigate the effects of boundary layer thickness and to a limited degree the velocity profile effect on boattail drag, an isolated boattail test was conducted in the NASA Lewis Research Center's 8×6 Foot Wind Tunnel. Boundary layer thickness was varied by changing model length, and by using a series of slotted rings. Analytical studies were also conducted.

MODEL AND TEST PROCEDURE

A schematic drawing of the model is shown in Fig. 2(a), and a photograph of the model installed in the tunnel is shown in Fig. 2(b). An isolated 8.0 inch diameter model was used. The tests were all at 0^{o} angle of attack and covered a Mach number range from 0.6 to 0.95. As shown in Fig. 2, variations in approach boundary layer thickness were obtained by varying the model forebody length. Three different forebody lengths were used to obtain three different ranges of boundary layer thicknesses. Also flow distortion devices were used with all three model lengths to provide additional boundary layer thickness and to investigate the additional effect of changing the boundary layer velocity profile. The photograph in Fig. 2(b) shows the model with a typical distortion ring installed. A

schematic and the dimensions of the distortion rings are given in Fig. 2(c).

Moveable probes and fixed rakes were used to measure boundary layer flow profiles in the boattail region. Surface static pressures were measured along the entire length of the model with emphasis on the boattail region. Pressure drag was determined by integrating the measured pressures on the boattail. In addition, fluorescent mini-tufts located on the boattails were used to establish regions of separate flow.

The various boattail geometries tested are shown in Fig. 3. The number designation is determined from the geometry of the boattail. The first two digits represent the ratio of the radius at the shoulder to the radius of a full circular arc boattail with the same trailing edge angle (see Fig. 3). The second two digits represent the terminal boattail angle. A sharp cornered shoulder would have a radius ratio of 0.

Changing the length of the model and adding the slotted distortion rings produces significant changes in the approaching boundary layer. Figure 4 shows typical boundary layer velocity profiles just upstream of the boattail shoulder for the thickest and thinnest boundary layers tested at Mach 0.9. One profile results from the shortest model with no disturbances and the other profile is from the longest model with the distortion rings attached. This range of model configurations provides an almost 5 to 1 change in displacement thickness.

RESULTS

Figure 5 shows the effect of Mach number on boattail drag of the 6524 boattail on an 8 inch diameter forebody. Four curves are shown, corresponding to four different approach displacement thicknesses. This Mach number effect was typical of all the geometries tested. There is little or no influence of Mach number until values above Mach 0.85 are reached. Above this speed drag rise is encountered. As the displacement thickness decreases, the drag rise occurs at a slightly lower Mach number. In the drag rise region at a constant Mach number a higher drag results with a thinner displacement thickness. This same effect has been observed on previous tests with undistorted boundary

layers. Figure 6 shows data, taken from Ref. 6, from three independent tests all showing the same trend. These tests were done on the AGARD 15^{o} boattail which in the designation convention used here would be an approximate 7523 boattail. This geometry is similar to the 6524 boattail of Fig. 5. The data in Fig. 5 includes the added effect of distorting the boundary layer, although it appears to correlate with displacement thickness.

For all of the nozzles tested, boattail drag was found to be very sensitive to boundary layer changes at high Mach numbers (Fig. 7), but this effect is reduced at lower Mach numbers and in general shows no significant effect at Mach 0.6. Similar tests were also conducted on a 4.0 inch diameter model and the same results were found. The boundary layer was thickened by increasing model length and by adding the distortion rings. The effects of both of these changes are combined in Fig. 7. Different results might be expected from varying the boundary layer by these two methods, however, the data correlates well with just displacement thickness. The short clean model produced the thinnest boundary layer, the long clean model increased the thickness, the short model with the distortion rings increased it further, and the long model with the distortion rings produced the thickest boundary layer.

At Mach 0.6 there was no effect of boundary layer changes on boattail drag for all of the geometries except the 2524 boattail. With the exception of this boattail, there was only a small effect on the boattail pressures. A typical example is the 6524 geometry shown in Fig. 8. There is a slight increase in the pressures at the boattail shoulder and a decrease in the pressures on the aft boattail as displacement thickness increases. These effects are compensating and result in no appreciable change in boattail drag. Tuft pictures of the boattail flows for the thickest and thinnest boundary layers are shown in Fig. 9. No significant separation is seen in either case.

The one geometry that does show an effect at Mach 0.6 is the 2524 boattail. Two curves are shown in Fig. 7 for this boattail at Mach 0.6. The upper curve is for varying displacement thickness with the clean model. The lower curve is varying displacement thickness with the dis-

tortion rings on. Both cases show no significant effect of displacement thickness. The difference in drag level is due to adding the distortion rings. This boattail geometry at this Mach number was the only case where the effect of adding the distortion rings were discernible from the effect of changing model length. The pressure distributions for this boattail are shown in Fig. 10. Comparing the two clean model pressure distributions shows almost no change. Comparing the pressures on the two models with distortion rings shows some changes, but they are compensating, similar to those on the 6524 boattail in Fig. 8, and the net effect is no appreciable change in drag. However, when comparing the configuration with and without the distortion rings, large pressure changes are seen. The major change is on the aft boattail where the models with distortion rings show recompression to higher levels. Examination of the tuft pictures in Fig. 11 shows a significant change in the region of separated flow. The dashed line denotes the beginning of increased tuft movement or increased turbulent flow. The solid line denotes the region where the tufts point upstream indicating reverse flow typical of a separated region. There is less separation on the model with the distorted boundary layer which would result in higher pressures on the aft boattail. Adding the distortion rings had the favorable effect of decreasing the amount of separation and lowering drag. The other geometries did not exhibit any significant separation at this Mach number and therefore showed no change in drag when the distortion rings were added. If appreciable regions of separated flow were present, changes in drag were always observed with changing boundary layer thickness.

There is a very significant effect of changing boundary layer characteristics on boattail drag at Mach 0.9. All of the different boattail geometries show this effect. In Fig. 7 the trend seen for any one boattail geometry includes results from models with and without the distortion rings. For every boattail geometry the pressure drag correlates well with displacement thickness, whether displacement thickness changed because of a different model length or the addition of a distortion ring. These drag changes at Mach 0.9 are the result of changes in the overexpansion pressures at the boattail shoulder and changes in the separated

flow pressures on the aft boattail. All of the boattail geometries tested exhibited some flow separation at Mach 0.9.

At Mach 0.9, as at Mach 0.6, the drag changes on the 2524 boattail are related to changes in separated flow. The pressure distributions on this boattail at Mach 0.9 are presented in Fig. 12. Some small changes are evident at the shoulder, but these are insignificant compared to the large changes on the aft boattail. There is a progressive increase in the pressures as the displacement thickness grows. The tuft pictures in Fig. 13 indicate significant changes in the separated flow regions. The separation is probably shock induced. A steep pressure rise is seen near the boattail shoulder. The thickest boundary layer appears to spread the pressure rise in this region and the shock may be weakened. With this thick boundary layer the separation point has moved further aft on the boattail as seen in Fig. 13. With the thicker boundary layer the amount of separated flow is diminished allowing more recompression and the higher pressures on the aft boattail produce less drag.

In general, for all of the boattail geometries, if separation is present large drag changes are seen with varying displacement thickness. If separation is not present this effect is not found.

Figure 14 shows the pressure distributions of the 6524 geometry at Mach 0.9. Again there are changes in the aft boattail pressures similar to that on the 2524 boattail geometry. The tuft pictures in Fig. 15 also show a significant change in the separated flow. This boattail shows a significant change in pressures at the boattail shoulder. The thinner boundary layer results in lower pressures at the shoulder, which also would produce higher drag. Without the separation on the aft boattail, the low pressures at the shoulder might have been offset by higher pressures on the aft boattail as was seen at Mach 0.6. However, the separation prevents this from occurring and the end result is a large drag change.

Further investigation of Fig. 7 shows that the geometry which exhibited the largest drag change was the 0016 boattail at Mach 0.9. This geometry has a sharp corner at the shoulder instead of the more gradual turning of the other geometries and terminates in only a 16^{o} angle. The

pressure distributions on this boattail are presented in Fig. 16. Only small differences are seen at the shoulder. However, on the remainder of the boattail the pressures are very sensitive to the changing boundary layer. As the displacement thickness gets larger the aft boattail pressures increase. Even with the large differences in pressure level none of the four curves has a shape that when considered alone would indicate an obvious separated flow case. The tuft pictures in Fig. 17, however, indicate very turbulent and separated flow. The thin boundary layer configuration has tufts indicating reverse flow up very near the shoulder and the flow appears separated over the entire boattail. The tuft pictures for the thick boundary layer, although indicating a very turbulent flow does not indicate any reverse flow. The separation change for this boattail is different than that seen on the other boattails. The rounded shoulder boattails have a separation point that appears to move longitudinally with displacement thickness. However, with the sharp corner boattail, the separation point is apparently fixed near the corner, but the character or nature of the flow changes. For the thickest boundary layer the boattail flow is very turbulent, but probably attached. As the boundary layer becomes thinner the turbulent intensity increases building to some flow reversal and separated flow.

Figure 18 compares the trend of boattail drag with displacement thickness determined from the 8×6 wind tunnel tests with that from four other studies on an AGARD 15^{o} boattail (Ref. 6) at Mach 0.9. This AGARD boattail had a radius ratio of 0.75 with a 23^{o} terminal angle (7523 designation). The AGARD data is compared against the boattail geometry that was the most similar to it (the 6524 boattail). Although the AGARD data does not extend over as wide a range of displacement thickness, the same trends as observed in this investigation can be seen. In general there is a significant decrease in boattail drag with increasing displacement thickness. For the AGARD data, the boundary layer displacement thickness was varied by changing model length or thinning the boundary layer with boundary layer injection.

An analytical study of the flow over these boattails was also performed. The analysis used in this study (Fig. 19) is a viscid-inviscid

interaction procedure based on the method of Ref. 14. The effects of the viscous layer near the body on the inviscid flow are taken into account by adding the displacement thickness onto the original geometry. The turbulent boundary layer analysis and the outer inviscid flow is calculated by a finite difference relaxation solution of the full transonic potential equation. In Fig. 20 is shown a comparison of the experimental and analytical boattail drags at both Mach 0.9 and 0.6 for the 6524 boattail. Although the absolute levels are different the analysis predicts essentially the same trend with increasing boundary layer thickness. The discrepancy in drag level is due to higher pressures on the aft boattail in the analytical results. Further work is required to improve the capability of the analysis when the flow has extensive region of separated flow.

CONCLUSIONS

A series of wind tunnel tests were conducted to investigate the effect of boundary layer thickness and shape on boattail drag. Several rounded shoulder boattail geometries and one sharp shoulder geometry were tested on an 8.0 inch diameter isolated model. The boundary layer was modified by changing model length and by adding boundary layer distortion devices. An analytical study on the same geometries was also conducted. The following results were obtained:

1. Changes in boundary layer displacement thickness resulted in significant changes in boattail drag at Mach 0.9, but had little effect at Mach 0.6.

2. At Mach 0.9 increasing boundary layer displacement thickness in general:

   a. resulted in higher pressures at the boattail shoulder.
   b. resulted in less separation on the aft boattail and therefore higher pressures in this region.
   c. significantly reduced boattail drag.

3. At Mach 0.6 increasing boundary layer displacement thickness on boattails with no significant separation

   a. increased the pressures at the boattail shoulder.
   b. decreased the pressures on the aft boattail.
   c. produced little change in drag.

LIST OF SYMBOLS

A_{max}	maximum cross-sectional area, 324.29 cm^2 (50.27 in^2)
b	distortion ring slot width, cm (in.)
C_d	boattail pressure drag coefficient, drag/$q_0 A_{max}$
C_p	pressure coefficient, $(p - p_0)/q_0$
c	distortion ring slot depth, cm (in.)
d	model diameter, 20.32 cm (8.00 in.)
h	distortion ring height, cm (in.)
L	model length, cm (in.)
L_1	distance from distortion ring to the boattail shoulder, cm (in.)
l	boattail nozzle length, cm (in.)
M_0	free stream Mach number
p	local static pressure, N/m^2 abs (psia)
p_0	free stream static pressure, N/m^2 abs (psia)
q_0	free stream dynamic pressure, $0.7\, p_0 M_0^2$, N/m^2 abs (psia)
R	radius at boattail shoulder, cm (in.)
R_c	radius of a full circular arc boattail, cm (in.)
V_l	local velocity, m/sec (ft/sec)
$V_{l_{max}}$	maximum local velocity, m/sec (ft/sec)
w	distortion ring slot spacing, cm (in.)
x	axial distance from boattail shoulder, cm (in.)
y	distance measured out from and perpendicular to the boattail surface, cm (in.)
β	trailing edge boattail angle, deg.
δ	displacement thickness, cm (in.)

REFERENCES

1. Chamberlin, R., "Flight Investigation of 24° Boattail Nozzle Drag at Varying Subsonic Flight Conditions," TM X-2626, 1972, NASA.

2. Chamberlin, R. and Blaha, B. J., "Flight and Wind Tunnel Investigation of the Effects of Reynolds Number on Installed Boattail Drag at Subsonic Speeds," AIAA Paper 73-139, Jan. 1973, Washington, D.C.

3. Chamberlin, R., "Flight Reynolds Number Effects on a Contoured Boattail Nozzle at Subsonic Speeds," TM X-3053, 1974, NASA.

4. Chamberlin, R., "Flight Reynolds Number Effects on a Fighter-Type, Circulat-Arc 19° Conic Boattail Nozzle at Subsonic Speeds," TM X-3121, 1974, NASA.

5. Wilcox, F. and Chamberlin, R., "Reynolds Number Effects on Boattail Drag of Exhaust nozzles from Wind Tunnel and Flight Tests," Airframe/Propulsion Interference, AGARD-CP-150, Advisory Group for Aerospace Research and Development, 1975, pp. 21-1 to 21-15.

6. Zonars, Dr. D., et al., "Effects of Varying Reynolds Number and Boundary Layer Displacement Thickness on the External Flow Over Nozzle Boattails," Improved Nozzle Testing Techniques in Transonic Flow, AGARD-AG-208, Advisory Group for Aerospace Research and Development, Paris (France); 1974, pp. 1-F1 to 1-F28.

7. Dansby, T., "Reynolds Number Effects on the Boattail Characteristics of a Simulated Nacelle at a Mach Number of 0.8," LG74ER0078, Oct. 1974, Lockheed-Georgia Co., Marietta.

8. Robinson, C. E. and Price, E. A., "Effect of Reynolds Number on the Nozzle Afterbody Performance of the Agard Nozzle Afterbody and the B-1 0.06-Scale Model at Transonic Mach Numbers," AIAA Paper 75-1321, Oct. 1975, Anaheim, Calif.

9. Reubush, D. E., "The Effect of Reynolds Number on Boattail Drag," AIAA Paper 75-63, Jan. 1975, Pasadena, Calif.

10. Reubush, D. E., "The Effect of Reynolds Number on the Boattail Drag of Two Wing Body Configurations," AIAA Paper 75-1294, Oct. 1975, Anaheim, Calif.

11. Laughrey, J. A., "Comparison of Testing Techniques for Isolated Axisymmetric Exhaust Nozzles in Transonic Flow," AIAA Paper 75-1292, Oct. 1975, Anaheim, Calif.

12. Fanning, A. E. and Glidewell, R. J., "Reynolds Number Effect on Nozzle Afterbody Throttle-Dependent Pressure Forces," AIAA Paper 75-1295, Oct. 1975, Anaheim, Calif.

13. Presz, W. M., Jr. and Pitkin, E. T., "Flow Separation Over Axisymmetric Afterbody Models," AIAA Paper 74-17, Feb. 1974, Washington, D.C.

14. Chow, W. L., Bober, L. J., and Anderson, B. H., "Numerical Calculation of Transonic Boattail Flow," TN D-7984, 1975, NASA.

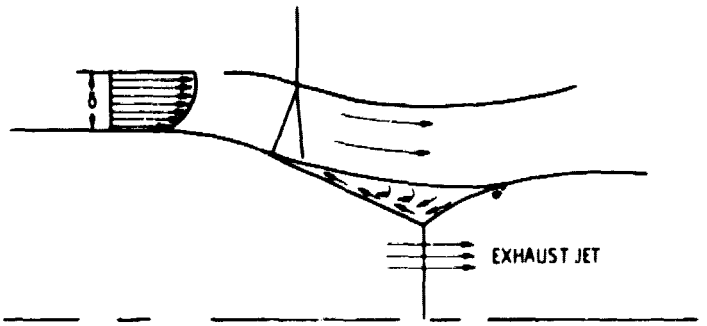

BOUNDARY LAYER THICKNESS
VELOCITY PROFILE
SHOCKS
SEPARATION
JET EFFECTS

Figure 1. - Aerodynamic factors influencing boattail drag.

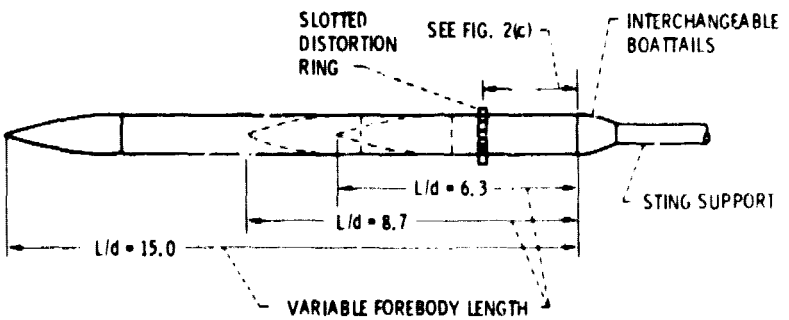

(a) MODEL SCHEMATIC.

Figure 2. - Axisymmetric model for isolated boattail drag test.

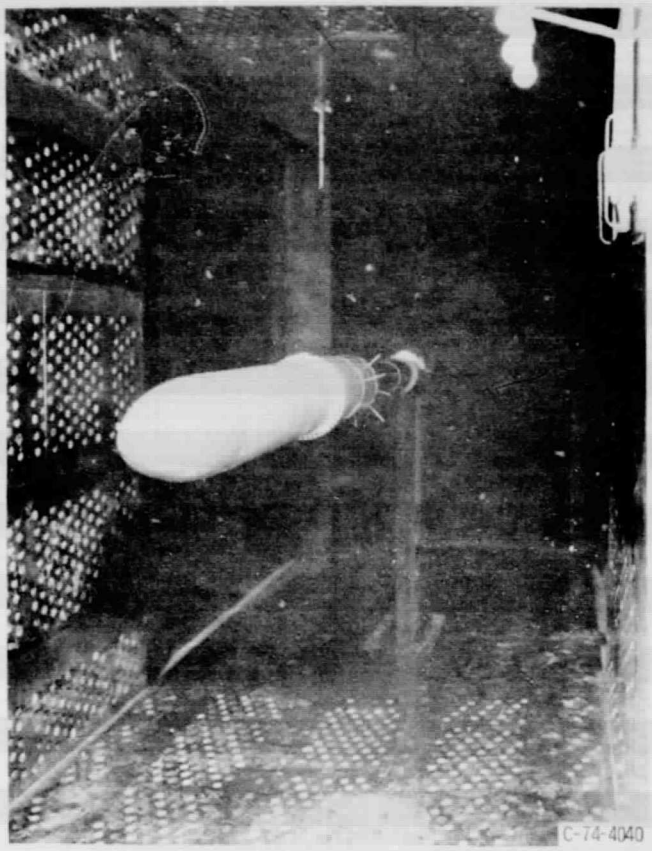

(b) PHOTOGRAPH OF MODEL IN 8 x 6 SWT.

Figure 2. - Continued.

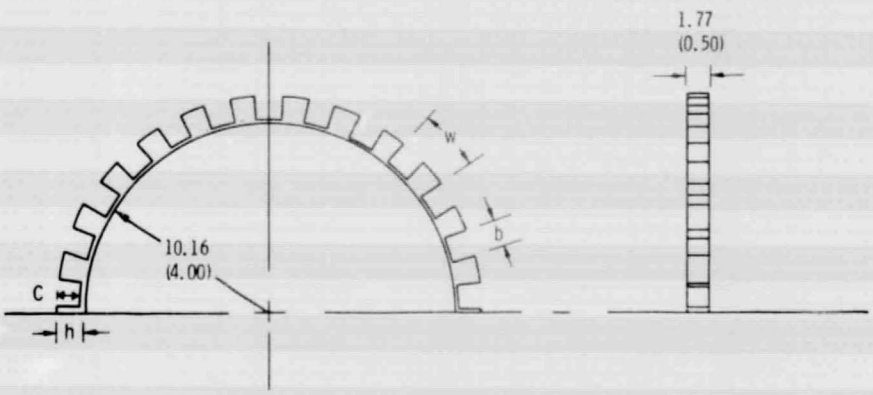

MODEL LENGTH, L/d	L_1/d	h/d	L_1/h	c/d	w/d	b/d
6.3	1.219	0.0375	32.5	0.0275	0.0351	0.0195
8.?	1.625	.050	32.5	.0375	.0468	.0234
15.0	2.438	.075	32.5	.0700	.0703	.0351

(c) DISTORTION RING DIMENSIONS.

Figure 2. - Concluded.

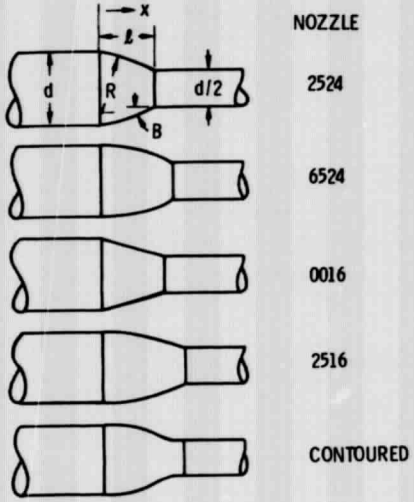

β, DEG	R/R_c	R_c/d	DESIGNATION
24	0.25	2.89	2524
24	0.65	2.89	6524
16	0	6.45	0016
16	0.25	6.45	2516
~ 30 MAX	(SEE REF. 3)		CONTOURED

Figure 3. - Boattail configurations tested.

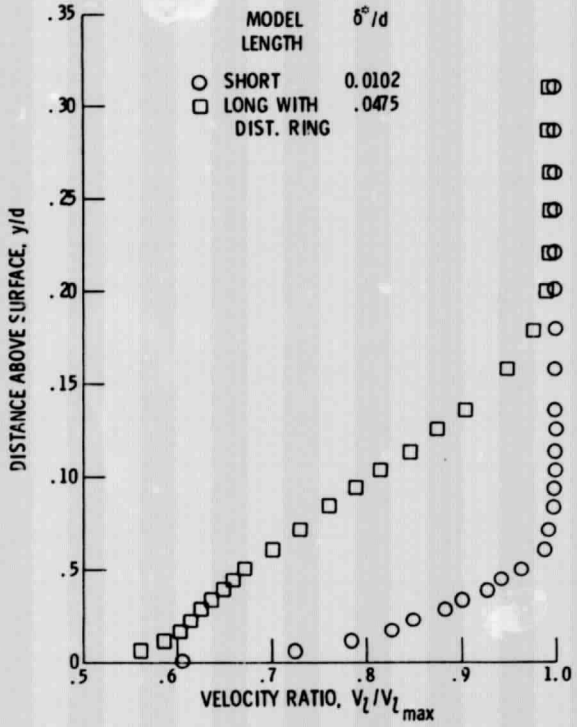

Figure 4. - Boundary layer velocity profile just upstream of boattail shoulder; 2524 boattail, $M_0 = 0.9$.

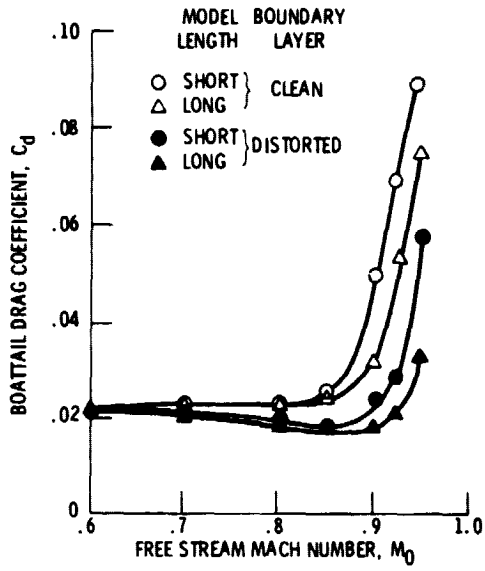

Figure 5. - Boattail drag as a function of free-stream Mach number; 6524 boattail.

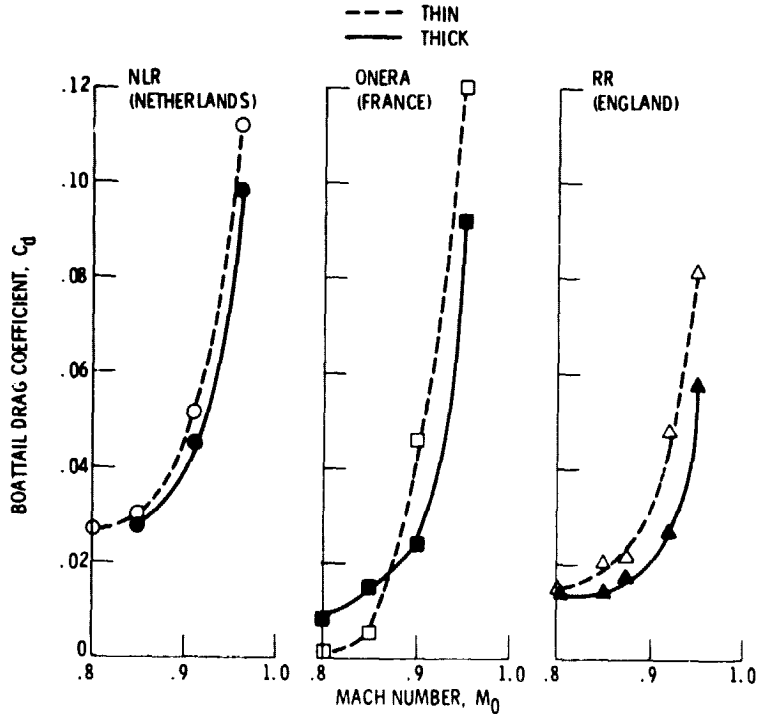

Figure 6. - Effect of Mach number on AGARD 15^0 boattail drag (data from ref. 6).

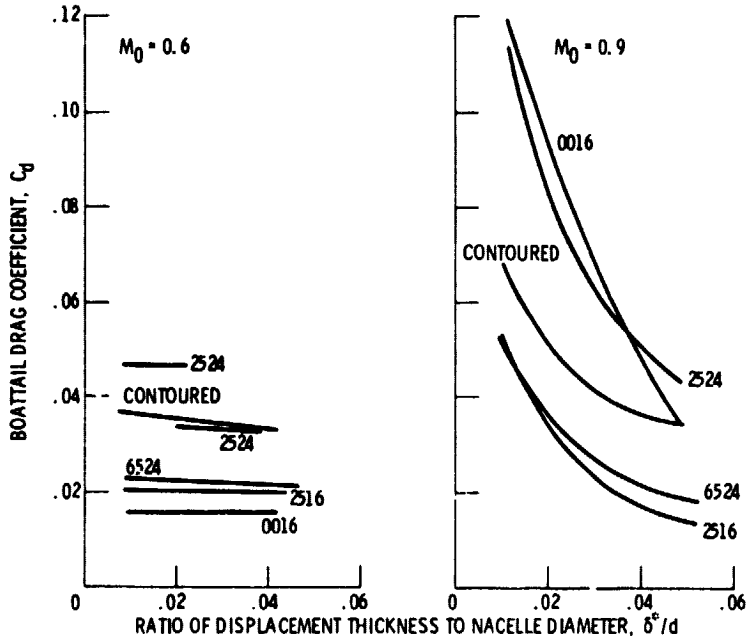

Figure 7. - Effect of boundary layer displacement thickness on boattail drag.

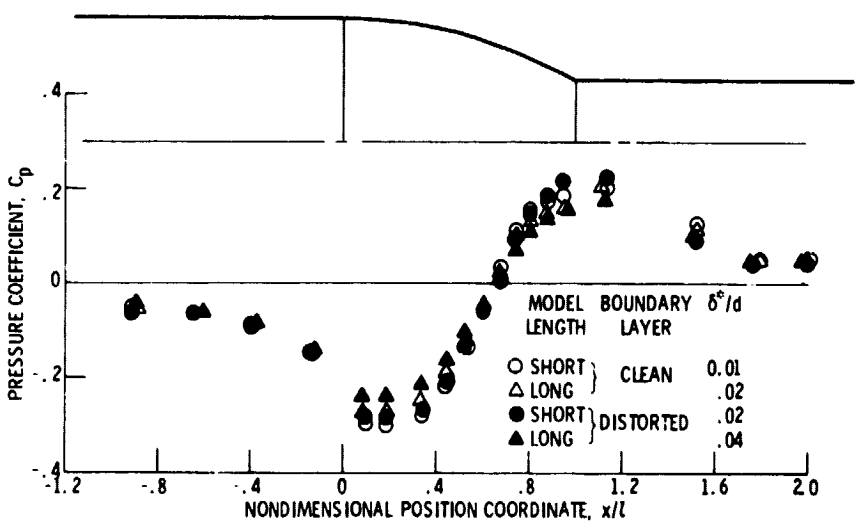

Figure 8. - Effect of boundary layer thickness on the 6524 boattail pressures, M_0 = 0.6.

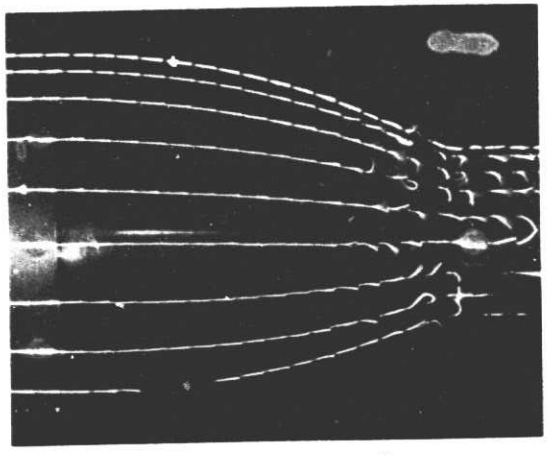

(a) DISPLACEMENT THICKNESS, $\delta^*/d = 0.01$.

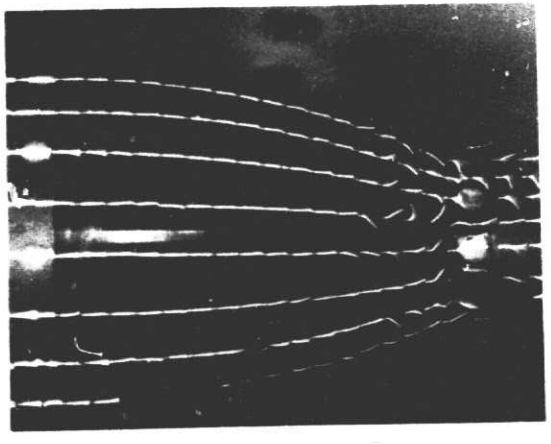

(b) DISPLACEMENT THICKNESS, $\delta^*/d = 0.04$.

Figure 9. - Tuft pictures of flow over the 6524 boattail; $M_0 = 0.6$.

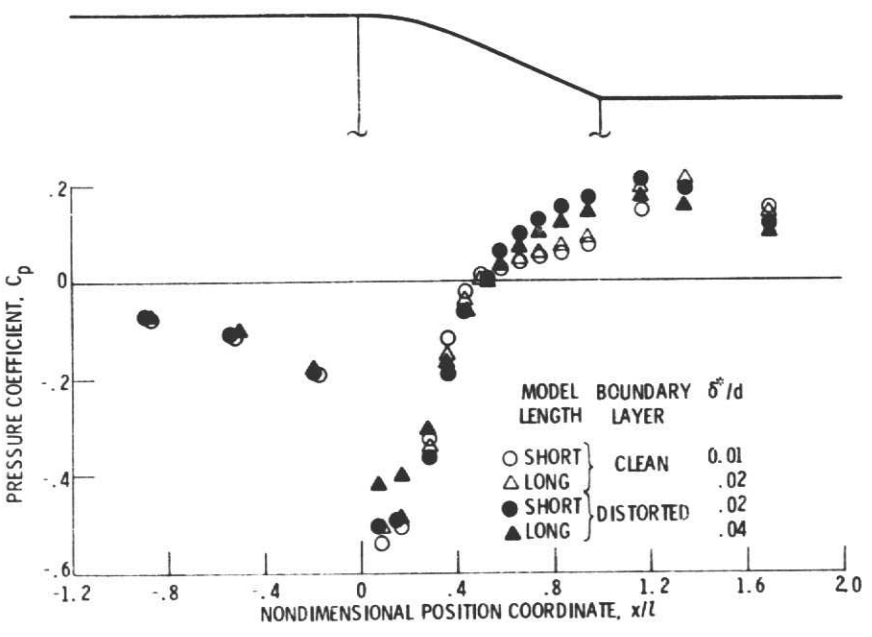

Figure 10. - Effect of boundary layer thickness on the 2524 boattail pressures, $M_0 = 0.6$.

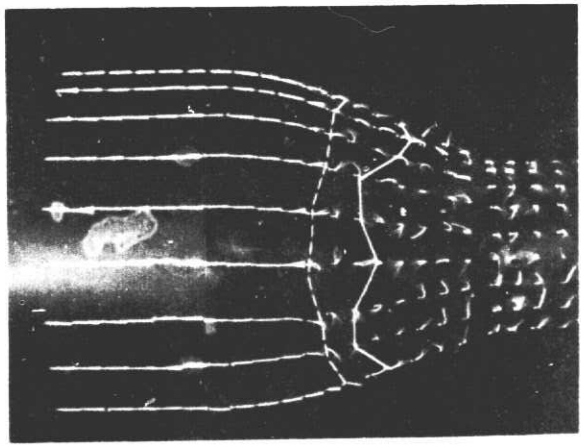

(a) DISPLACEMENT THICKNESS, $\delta^*/d = 0.01$.

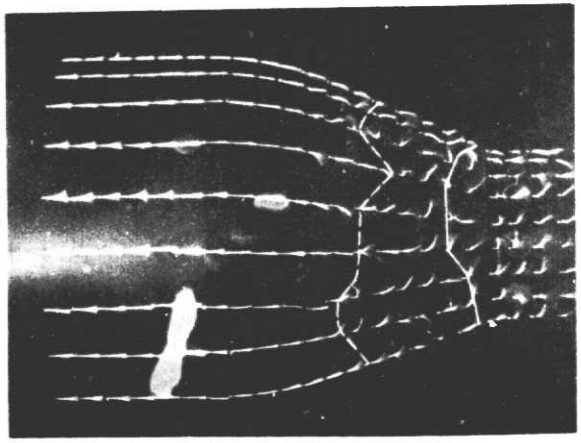

(b) DISPLACEMENT THICKNESS, $\delta^*/d = 0.04$.

Figure 11. - Tuft pictures of flow over the 2524 boattail; $M_0 = 0.6$. Solid line - reversed flow, separation; dashed line - highly turbulent flow.

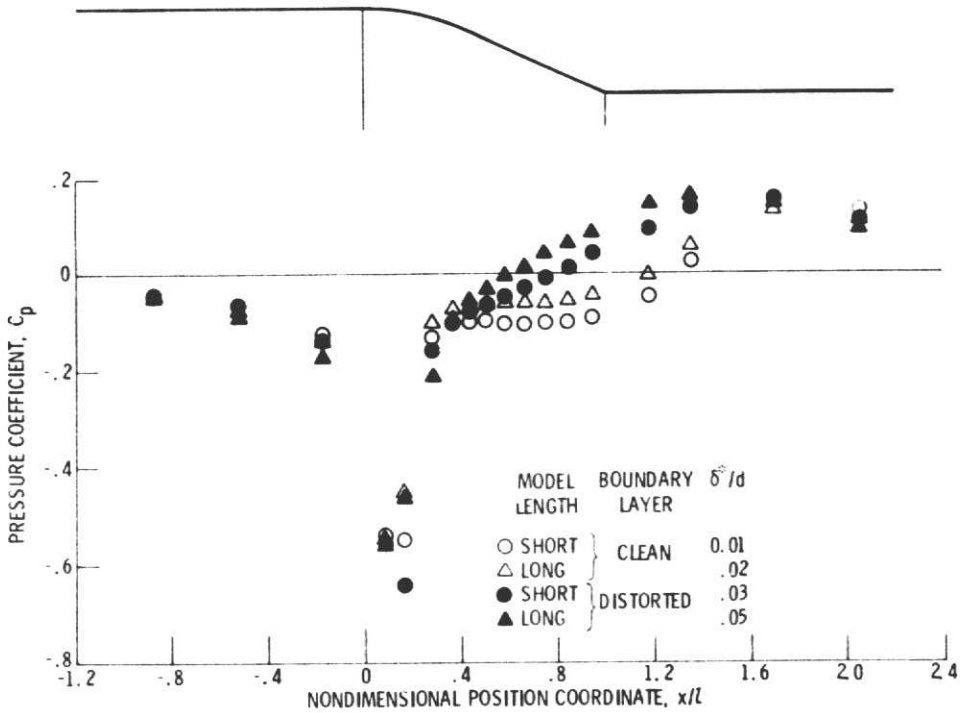

Figure 12. - Effect of boundary layer thickness on the 2524 boattail pressures, $M_0 = 0.9$.

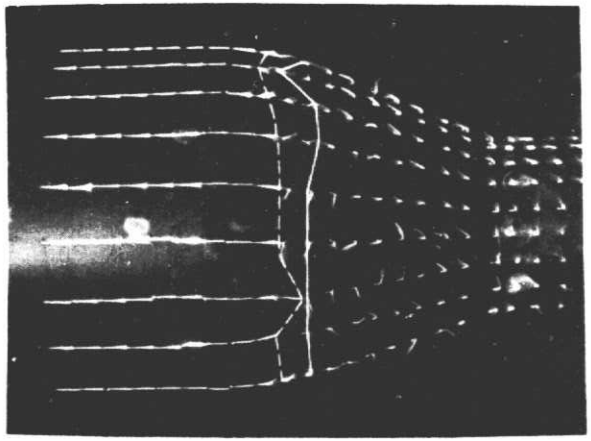

(a) DISPLACEMENT THICKNESS, $\delta^*/d = 0.01$.

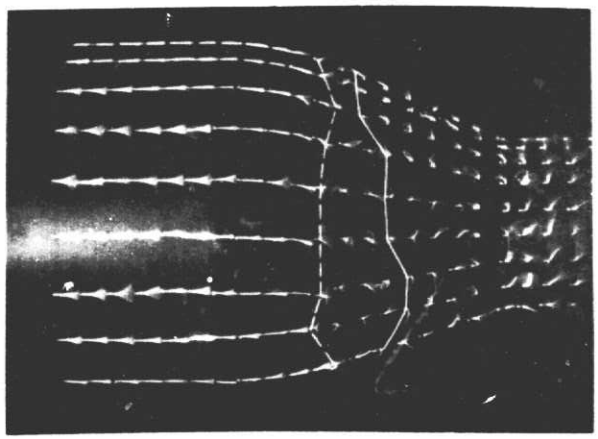

(b) DISPLACEMENT THICKNESS, $\delta^*/d = 0.05$.

Figure 13. - Tuft pictures of flow over the 2524 boattail; $M_0 = 0.9$. Solid line - reversed flow, separation; dashed line - highly turbulent flow.

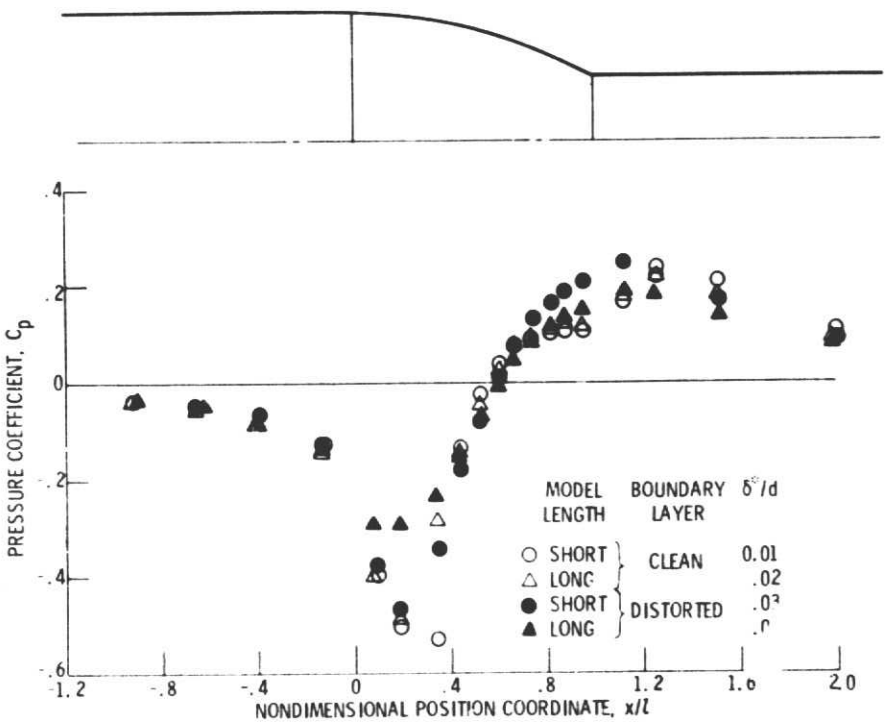

Figure 14. - Effect of boundary layer thickness on the 6524 boattail pressures, $M_0 = 0.9$

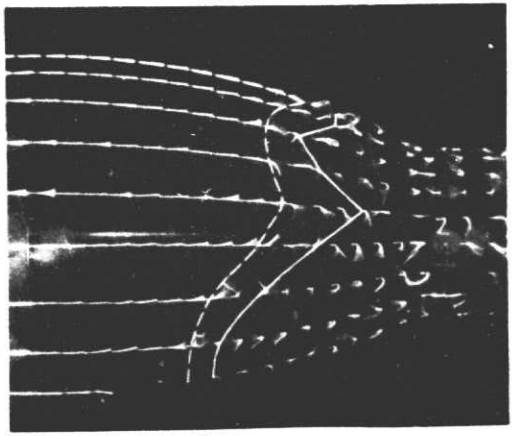

(a) DISPLACEMENT THICKNESS, $\delta^*/d = 0.01$.

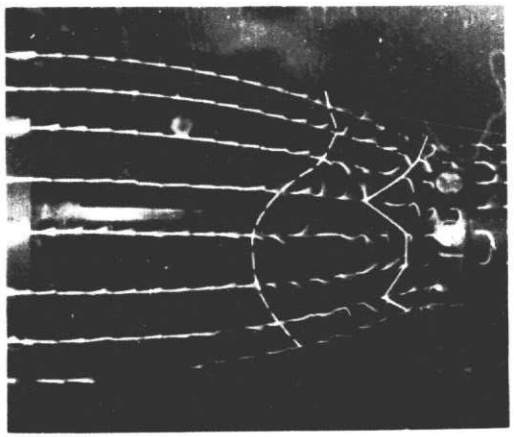

(b) DISPLACEMENT THICKNESS, $\delta^*/d = 0.05$.

Figure 15. - Tuft pictures of flow over the 6524 boattail; $M_0 = 0.9$. Solid line - reversed flow; separation; dashed line - highly turbulent flow.

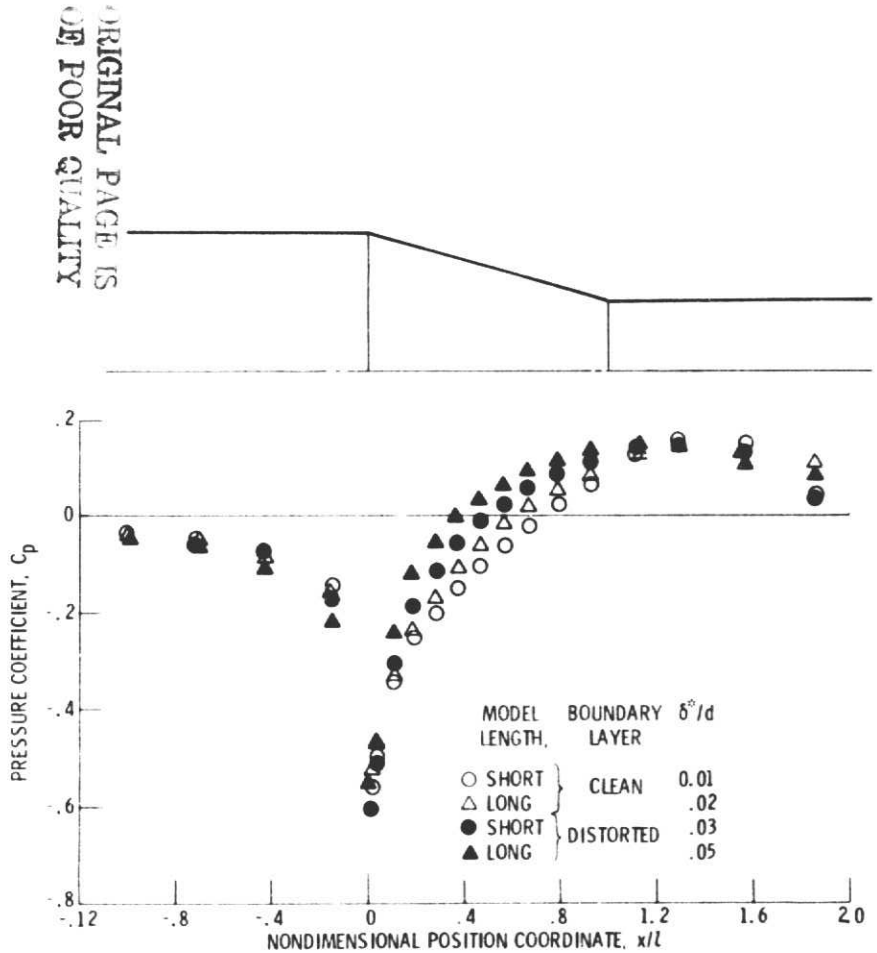

Figure 16. - Effect of boundary layer thickness on the 0016 boattail pressures, $M_0 = 0.9$.

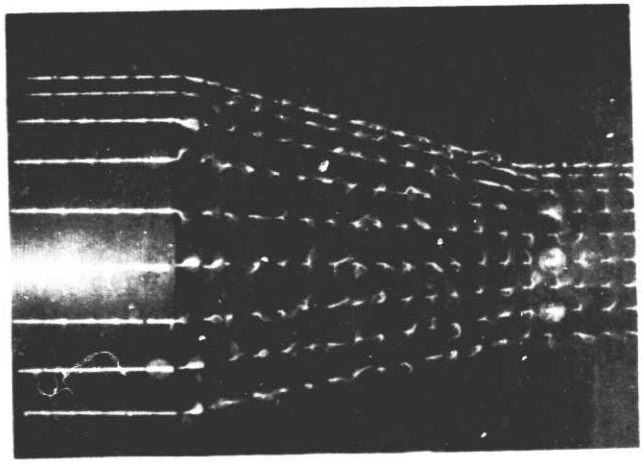

(a) DISPLACEMENT THICKNESS, $\delta^*/d = 0.01$.

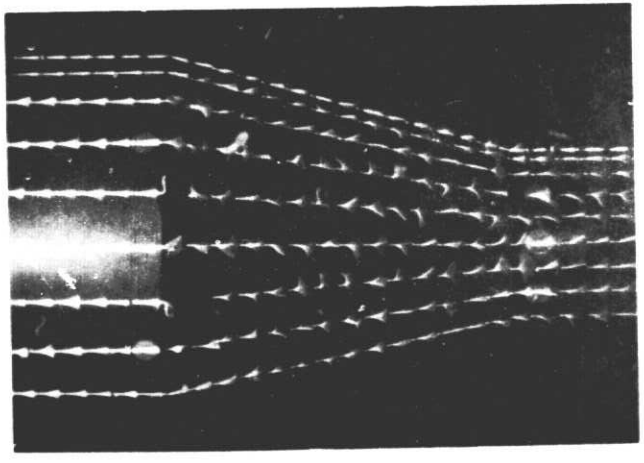

(b) DISPLACEMENT THICKNESS, $\delta^*/d = 0.05$.

Figure 17. - Tuft pictures of flow over the 0016 boattail; $M_0 = 0.9$.

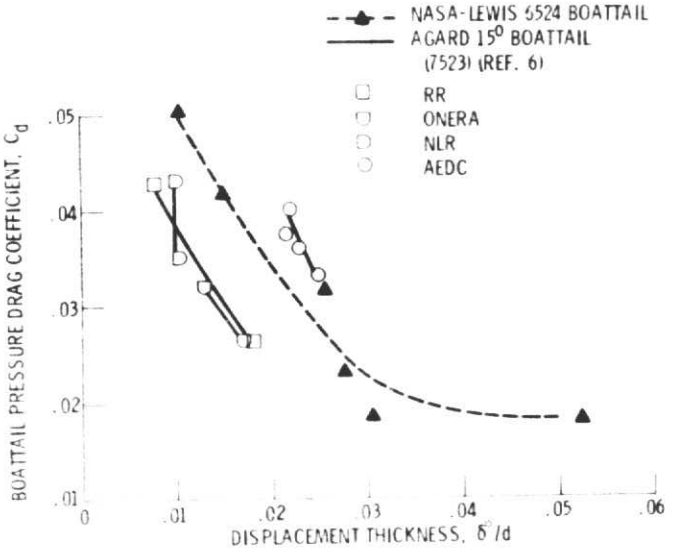

Figure 18. - Comparison of results from several different tests, $M_0 = 0.9$.

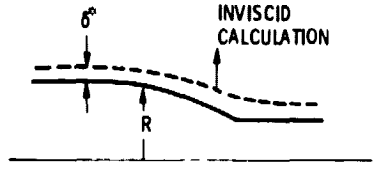

INVISCID: TRANSONIC FINITE DIFFERENCE, RELAXATION
VISCOUS: TURBULENT, INTEGRAL
COUPLING: INVISCID FLOW BOUNDARY CONDITION OBTAINED FROM R + δ*

Figure 19. - Transonic boattail analysis.

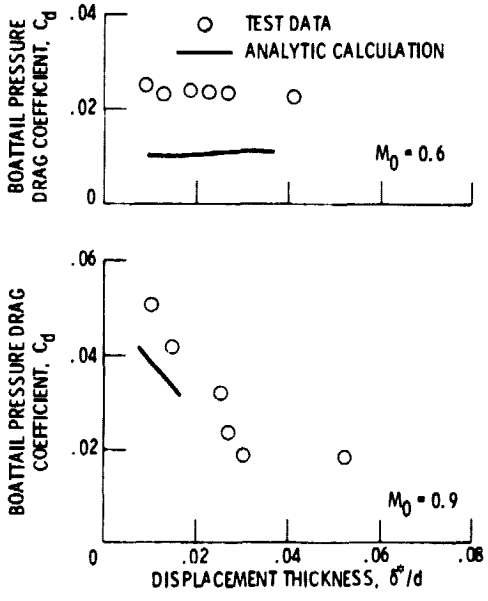

Figure 20. - Comparison of analytic and experimental pressure drag 6524 boattail geometry.